Naval Research Laboratory

Washington, DC 20375-5320

NRL/MR/6134--20-10,038

Characterizing Oxygen Reduction Catalysis on Stainless Steel Oxides

Rachel M. Anderson
Carlos M. Hangarter
Matthew J. Strom
Steven A. Policastro

Center for Corrosion Science and Engineering Branch
Chemistry Division

February 24, 2020

REPORT DOCUMENTATION PAGE

Form Approved
OMB No. 0704-0188

1. REPORT DATE *(DD-MM-YYYY)*	**2. REPORT TYPE**	**3. DATES COVERED** *(From - To)*
24-02-2020	NRL Memorandum Report	October 2018 – September 2019

4. TITLE AND SUBTITLE

Characterizing Oxygen Reduction Catalysis on Stainless Steel Oxides

5a. CONTRACT NUMBER

5b. GRANT NUMBER

5c. PROGRAM ELEMENT NUMBER
NISE

6. AUTHOR(S)

Rachel M. Anderson, Carlos M. Hangarter, Matthew J. Strom, and Steven A. Policastro

5d. PROJECT NUMBER

5e. TASK NUMBER

5f. WORK UNIT NUMBER
N2R6

7. PERFORMING ORGANIZATION NAME(S) AND ADDRESS(ES)

Naval Research Laboratory
4555 Overlook Avenue, SW
Washington, DC 20375-5320

8. PERFORMING ORGANIZATION REPORT NUMBER

NRL/MR/6134--20-10,038

9. SPONSORING / MONITORING AGENCY NAME(S) AND ADDRESS(ES)

Naval Research Laboratory
4555 Overlook Avenue, SW
Washington, DC 20375-5320

10. SPONSOR / MONITOR'S ACRONYM(S)

NRL-NISE

11. SPONSOR / MONITOR'S REPORT NUMBER(S)

12. DISTRIBUTION / AVAILABILITY STATEMENT

DISTRIBUTION STATEMENT A: Approved for public release; distribution is unlimited.

13. SUPPLEMENTARY NOTES

Karles Fellowship

14. ABSTRACT

In this report the characterization and electrochemical behavior of a Navy-relevant stainless steel alloy is summarized. A UNS S13800 stainless steel alloy was compared to a model binary alloy (FeCr 80:20 wt%), as well as its constituent pure components, in order to determine the relevant catalytic species for the oxygen reduction reaction. The oxygen reduction reaction is an important reaction in galvanic corrosion. Electrochemical and surface analytical techniques gave insight into the role of the oxide composition on the electrochemical properties. It was found that enrichment of chromium occurs near the surface, but both iron and chromium species are present on the outer surface oxide layer. The iron affected the impedance characteristic of the more insulating chromium oxide layer. There was a coincident increase in the capacitance of the passive film and oxidation state change of the iron species where the stainless steel alloy becomes active for the oxygen reduction reaction. These studies suggest that the oxidation state of the iron determines the oxygen reduction reaction behavior of a stainless steel. Understanding the relationship between the stainless steel alloy composition and the oxygen reduction reaction behavior is important for the development of a broad model for the electrochemical behavior of stainless steels in galvanic corrosion systems.

15. SUBJECT TERMS

Corrosion Stainless steel Oxygen reduction reaction

16. SECURITY CLASSIFICATION OF:			**17. LIMITATION OF ABSTRACT**	**18. NUMBER OF PAGES**	**19a. NAME OF RESPONSIBLE PERSON**
					Rachel M. Anderson
a. REPORT	**b. ABSTRACT**	**c. THIS PAGE**	Unclassified Unlimited	22	**19b. TELEPHONE NUMBER** *(include area code)*
Unclassified Unlimited	Unclassified Unlimited	Unclassified Unlimited			(202) 404-6044

Standard Form 298 (Rev. 8-98)
Prescribed by ANSI Std. Z39.18

This page intentionally left blank.

CONTENTS

FIGURES

TABLES

EXECUTIVE SUMMARY

In this report, the characterization and electrochemical behavior of a Navy-relevant stainless steel alloy is summarized. A UNS S13800 stainless steel alloy was compared to a model binary alloy (FeCr 80:20 wt%), as well as its constituent pure components, in order to determine the relevant catalytic species for the oxygen reduction reaction. The oxygen reduction reaction is an important reaction in galvanic corrosion. Electochemical and surface analytical techniques gave insight into the role of the oxide composition on the electrochemical properties. It was found that enrichment of chromium occurs near the surface, but both iron and chromium species are present on the outer surface oxide layer. The iron affected the impedance characteristic of the more insulating chromium oxide layer. There was a coincident increase in the capacitance of the passive film and oxidation state change of the iron species where the stainless steel alloy becomes active for the oxygen reduction reaction. These studies suggest that the oxidation state of the iron determines the oxygen reduction reaction behavior of a stainless steel. This could be due to either changes in oxygen adsorption energies, or to resultant changes in resistance of the insulting chromium surface oxide. Understanding the relationship between the stainless steel alloy composition and the oxygen reduction reaction behavior is important for the development of a broad model for the electrochemical behavior of stainless steels in galvanic corrosion systems.

This report presents research conducted by Rachel M. Anderson, Carlos M. Hangarter, Matthew J. Strom, and Steven A. Policastro.

This page intentionally left blank.

CHARACTERIZING OXYGEN REDUCTION CATALYSIS ON STAINLESS STEEL OXIDES

1. INTRODUCTION

1.1 Background

The oxygen reduction reaction (ORR) on stainless steel oxides is a complex process that can drive galvanic corrosion on more electrochemically active materials such as aluminum, as well as drive localized corrosion. The goal of this research is to relate oxide composition and thickness to reaction kinetics for the ORR on stainless steel oxides. A passive chromium-rich oxide film forms on stainless steels at more positive potentials [1-2], and its corrosion behavior has been extensively studied in terms of charge transfer across a resistive film [3]. However, the oxide/oxy-hydroxide and partially-reduced surface is different and not well understood at more negative potentials, and it is the structure and composition of the oxide in this potential region that is of interest for ORR catalysis in a galvanic couple [4]. The challenge of this problem is partly associated with the nanometer thickness of these films, as well as the difficulty in characterizing lateral features inherent to structural alloys such as stainless steel. The local structure of the oxide, including defects and variations in composition and microstructure, contributes to the catalytic properties of the surface, and importantly this local oxide structure changes with potential [2].

In atmospheric environments thin film aqueous electrolytes can form [5] that are characterized by film thicknesses that are on the order of, or thinner than, the concentration depletion region for dissolved oxygen in an aqueous solution. Because of this high flux of oxygen, the corresponding cathodic reduction kinetics become increasingly important in driving galvanic corrosion. Previous studies of galvanic coupling to aluminum in an atmospheric environment have shown that significantly more damage was found at the stainless steel fastener materials, as opposed to titanium, even though titanium is the more noble metal [6]. While two materials might have similar open circuit potential (OCP) values, the kinetics for the relevant cathodic reactions can vary significantly. Figure 1 demonstrates this concept. Cathodic potentiodynamic polarization scans are shown in 0.6 M NaCl for Pt (the most noble), as well as pure titanium and UNS S31600 stainless steel. The titanium and the UNS S31600 have similar OCP values, but at value of -0.8 V_{SCE}, which is approximately the OCP value of a common aluminum alloy AA7075 and marked with a dashed line, the current density values vary by an order of magnitude. This represents faster ORR kinetics on the UNS S31600 and as a result a larger galvanic current leading to more aluminum oxidation. It is interesting to note that both titanium and stainless steel form a passive oxide at the surface of the metal. Rotating disk electrode experiments simulating thin film electrolytes found discrepancies between the limiting currents of Pt and stainless steel at high rotation rates [4]. This points to the role that the oxide plays in the ohmic drop of the entire system.

Manuscript approved February 10, 2020.

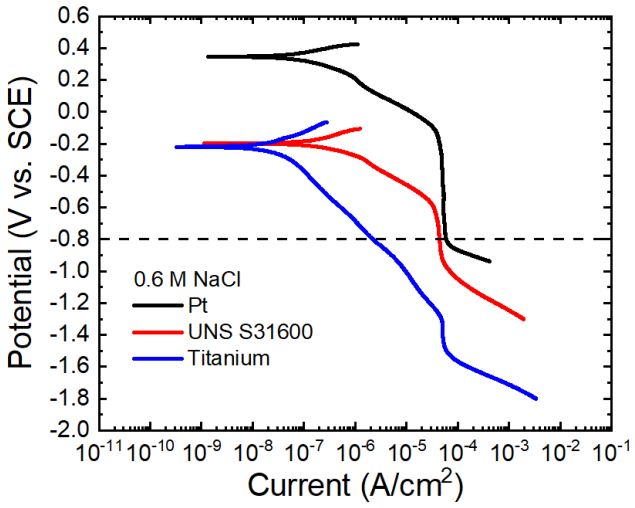

Figure 1 - Potentiodynamic polarization curves for pure Pt, UNS S13800 stainless steel, and pure titanium in 0.6 M NaCl with 900 s OCP, 1 mV/s scan rate, ambient aeration, 25°C.

The exposure conditions and history of the stainless steel determine the makeup of its surface oxide, and as a result its ability to drive corrosion on less noble materials. It is important to understand the connection between reaction conditions and the composition and properties of the surface layer in order to design corrosion mitigation strategies. A stainless steel oxide is a complex system for several reasons.

- First, the passive chromium (III) oxide layer forms an insulating barrier between the elemental metal and the electrolyte.
- Second, at the oxide-electrolyte interface, there may be iron ions with different valence values present that enhance electron tunneling through the oxide.
- Third, the ORR is an inner sphere reaction dependent on the adsorption of the reactant to the surface, therefore the chemical nature of the surface is important.

As a heterogeneous catalytic reaction, ORR is a highly surface-dependent process. The pretreatment of the stainless steel has been shown to have a significant impact on its catalytic behavior [7]. Cathodic pretreatment increases the rate of ORR, as does a freshly polished sample, and on a passivated surface the reduction of Fe_2O_3 occurs concurrently with ORR. Moffat et al. studied the electron transfer rate on pure chromium electrodes [8]. The electron transfer rate was found to exponentially depend on the thickness of the oxide. Another study examined well-defined Fe_3O_4 and γ-FeOOH electrodes as catalysts for O_2 reduction and the authors found that, 1) the presence of Fe^{2+} surface sites was necessary for ORR to occur and 2) these Fe^{2+} species affected the electrical conductivity of the oxide [9]. A recent study did an in-depth analysis of the effect of experimental parameters on the thickness and composition of a UNS S13800 stainless steel oxide [10]. This study showed that the oxygenation of the solution in which the electrode is immersed affects the composition of the oxide formed.

1.2 Approach

The local structure and chemical nature of the oxide determines the catalytic properties of the surface. As this structure changes with potential, *in situ electrochemical* studies are necessary to reveal the surface species present and their impact on reaction mechanisms and kinetics for the ORR. *Ex situ* surface analyses after potential holds provide valuable information, but are influenced by air oxidation.

Previous studies have emphasized that while *ex situ* studies of a thick anodized oxide are adequate, at more reducing potentials *ex situ* studies mainly characterize the air-formed oxide during the sample transfer to analysis chamber [11]. X-ray absorption spectroscopy (XAS) studies are ideally suited to probe this disordered oxide, and experiments can be performed under relevant reaction conditions for the ORR Previously, work concerning FeCr model alloys was performed in XAS transmission mode in which thin films were deposited on an x-ray transparent substrate [12-14]. While quantitative measurements about the material loss were obtained, and overall trends in oxidation state over time were determined, these measurements still probed the entire depth of the oxide (on the order of 100 nm). In this work, the goal is to move towards bulk engineering alloy samples in which the surface can be selectively probed.

Current *in situ* X-ray absorption techniques on bulk electrodes, such as fluorescence, have sample volumes with depths on the order of microns and the signal is often attenuated due to self-absorption [15]. Grazing incidence techniques allow for surface sensitivity but are subject to surface roughness and alignment limitations when attempting *in situ* electrochemical measurements. Total electron yield gives the desired surface sensitivity [16], but without the ability to study the material under electrochemical control. Some attempts have been made towards this goal of performing experiments outside of vacuum with conversion electron yield (CEY) or intermittent solution exposure [17-18]. Using the same principles as TEY and CEY, the technique proposed here uses the sample electrode in solution to collect the photoelectrons generated from the X-ray beam interacting with the sample. This approach has been previously suggested [19-20], but never collected and reported as XAS data in solution. In our approach, the passive film was held at a constant potential and studied *in situ*. Preliminary experiments of the X-ray absorption near edge structure (XANES) regions of both Fe and Cr show how challenging these *in situ* measurements are, but also are promising steps towards future experimental method development.

From a combination of electrochemical, *ex situ* surface analysis, and *in situ* XAS measurements, we can draw conclusions about the surface oxide composition and its ability to support the catalytic ORR. Together these measurements and analyses provide a comprehensive structural and compositional view of the surface to correlate with electrochemical properties. In the following stages of this work, these results are intended to be interpreted using insights gained from atomistic modeling studies of the complex oxide layer to determine the active species that drive corrosion.

2. EXPERIMENTAL APPROACH

2.1 Materials

2.1.1 Sample Fabrication

An Fe/Cr 80/20 wt% (99.95% pure) sputtering target was purchase from ACI Alloys Inc. Thin films on silicon wafers were obtained using an AJA sputtering system with an estimated sputtering rate of ~4 nm/min in an argon atmosphere (pressure 2.5 mTorr). Pure Cr and Fe targets were used in a Temescal e-beam evaporator system to deposit thin films (~100 nm) onto silicon wafers (<100> orientation, N type, 625 μm thick, University Wafer). Coupons of UNS S13800, pure Cr (99.99%) and pure Fe were also used in the electrochemical experiments and characterized using the various techniques described below.

2.2 Methods

2.2.1 Electrochemical Experiments

Potentiodynamic polarization curves were performed with the following protocol.

- For the thin metal films, the samples were used as fabricated with no further surface preparation.
- The bulk metal coupon sample surfaces were abraded to 1200 grit with SiC paper and polished using a 1 μm diamond suspension (potentiodynamic polarization scans and surface analysis) or 1 μm alumina (all other electrochemical tests).
- The samples were then sonicated in water, and rinsed with isopropyl alcohol and water before electrochemical tests.
- Electrical connection was made using a Cu clip to the front surface of the film that had been deposited on the silicon wafer.
- Electrochemical impedance spectroscopy (EIS) measurements were used to first ensure that good contact was made (high frequency resistance less than 30 Ω) before proceeding with the polarization or potentiostatic experiments.
- Cathodic polarization scans were performed using a saturated calomel reference electrode (SCE), and all potentials are reported versus this reference system. Cathodic polarizations scans were run in triplicate after an 18-hour open circuit equilibration. The electrolyte used was 0.6 M NaCl, and the scans began +20 mV versus the open circuit potential to -1.2 V_{SCE} at a scan rate of -0.167 mV/s. Gamry potentiostats were used and glass jacketed cells (Biologic) allowed for temperature control with an external water bath.
- Potentiostatic EIS measurements were conducted at 5 mV_{RMS} after 20 min potentiostatic holds for the metal coupon samples, or 1 h potentiostatic holds for the thin metal film FeCr sample.

2.2.2 Glow Discharge-Optical Emission Spectroscopy (GD-OES)

Glow discharge optical emission spectroscopy (GD-OES) measurements for elemental depth analysis were performed using a GD-Profiler 2 (Horiba) in the radiofrequency mode. A 4 mm anode was used with a power of 35 W and a pressure of 650 Pa. Quantification was possible through calibration with CRM materials, as well as pressed-pellet samples with Cu and salt additions to allow for determination of oxygen. An integrated differential interferometer was used to simultaneously determine depth during the measurement.

2.2.3 X-ray Photoelectron Spectroscopy (XPS)

X-ray photoelectron spectroscopy (XPS) was performed with a K-Alpha XPS system on both FeCr and UNS S13800 stainless steel samples. A monochromatic Al Kα X-ray source was used with a spot size of 400 μm diameter spot size. For high-resolution energy scans, a pass energy of 20 eV was used with a step size of 0.150 eV. A gold sample was used for calibration with an Au $4f_{7/2}$ metallic gold binding energy (BE) of 84.0 eV. Data analysis was performed using the CasaXPS software. A Shirley background subtraction was used for all high resolution elemental scans. After a potentiostatic hold of 3600 s, the samples were rinsed with water, dried with N_2, and transferred to the vacuum chamber of the XPS within ~15 min.

2.2.4 X-ray Absorption Spectroscopy (XAS)

XAS data were collected at the 8ID beamline at the National Synchrotron Light Source II at Brookhaven National Laboratory. For Pt and Au L3 edges, a mix of 1:1 He:N_2 was used in the I_0 ion chamber. Calibration was performed using a reference foil, then *in situ* electrochemical measurements were conducted with simultaneous electrochemical and fluorescence data collection using a passivated

implanted planar silicon (PIPS) detector). For the Fe and Cr edges, a mix of 5:1 He:N_2 was used in the I_0 ion chamber. A chopper at a frequency of 97 Hz was used with a multichannel lock-in amplifier to collect the signal from the potentiostat and the fluorescence signal. For the Pt electrode, a 2 mm disk electrode (Pine) was used with a final polish of 50 nm alumina in 0.l N H_2SO_4 (TraceMetal Grade, Fisher Scientific). The UNS S13800 stainless steel was a 5 mm disk electrode with a final polish of 1 µm diamond in 0.6 M NaCl solution.

3. RESULTS AND DISCUSSION

3.1 Electrochemical Studies

3.1.1 Potentiodynamic Polarization

Cathodic polarization curves in 0.6 M NaCl of the UNS S13800, FeCr, Fe and Cr samples are compared in Figure 2. While the FeCr has a ~120 mV more positive OCP, the potential regions over which the ORR is under activation control are similar for all of the materials and the samples reach the diffusion limited region for ORR at approximately the same potential, -600 mV. The difference in open circuit could be due to differences in alloying elements and the lack of microstructure on the FeCr thin film sample.

The pure chromium sample has an OCP value of ~-175 mV, similar to that of the UNS S13800. However, throughout the cathodic polarization curve, the currents measured are approximately a factor of 5 lower than that for the UNS S13800 or the FeCr.

Pure iron is not stable in this solution and is actively dissolving at its OCP. Because of this, the initial OCP hold was shortened to 1 hour. As the potential is swept negative, the iron sample is stabilized and by -700 mV has reached its diffusion limited ORR current and behaves consistently with the FeCr and UNS S13800 samples.

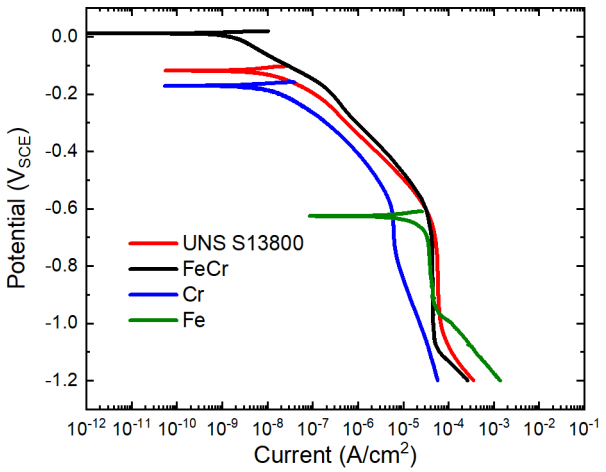

Figure 2 – Polarization curves of UNS S13800, FeCr, pure Fe and pure Cr in 0.6 M NaCl after 18 hour OCP (1 h for Fe).

3.1.2 Cyclic Voltammetry

Hysteresis in the ORR behavior with scan direction has been observed on both Fe and stainless steel samples, demonstrating the effect of potential on the oxide composition/ORR catalytic ability [21-22]. The history of the passive film and formation conditions affects the onset potential for ORR. Electrochemical cyclic voltammetry (CV) studies were performed on the different materials to observe the redox behavior of the surface species that is not apparent at slower scan rates.

Figure 3 contains CVs of UNS S13800 and the pure metals Fe, Cr and Ni. Beginning with the UNS S13800 scan (Figure 3a) multiple anodic and cathodic peaks are observed. Importantly, these scans are started after a 1 hour OCP hold in order for a stable passive film to develop. Beginning at OCP, the potential is swept negative (at 100 mV/s) and the ORR begins ~-600 mV, as is seen in the potentiodynamic polarization curves previously. However, with this faster scan rate, after the initial decrease in current due to diffusion of oxygen to the surface, there are additional cathodic peaks.

Another interesting feature is the repeatability of these scans. Upon cycling again, there is a slight decrease in cathodic current most likely due to the depletion of oxygen at the surface of the electrode and the faster scan rate, but overall the rest of the scans overlay. This implies that the surface species undergoing redox cycling are either stabilized, or regenerated in a controlled manner within this potential region. Figure 3b is the CV for pure Ni, and there is a clear oxidation peak for the Ni at ~-600 mV. Cr (Figure 3c) exhibits very low capacitance and no clear redox peaks within this potential region. Fe (Figure 3d) shows significant oxidation (dissolution) above the scan limit here of -700 mV. Both Ni and Fe have larger currents at the negative scan limit of -1200 mV, indicative of higher activity for the hydrogen evolution reaction (HER), or possibly cathodic dissolution in the case of Fe. Based on the Ni and Fe pure metal CVs, the cathodic and reduction peaks in the UNS S13800 CV can be assigned to some combination of these two species.

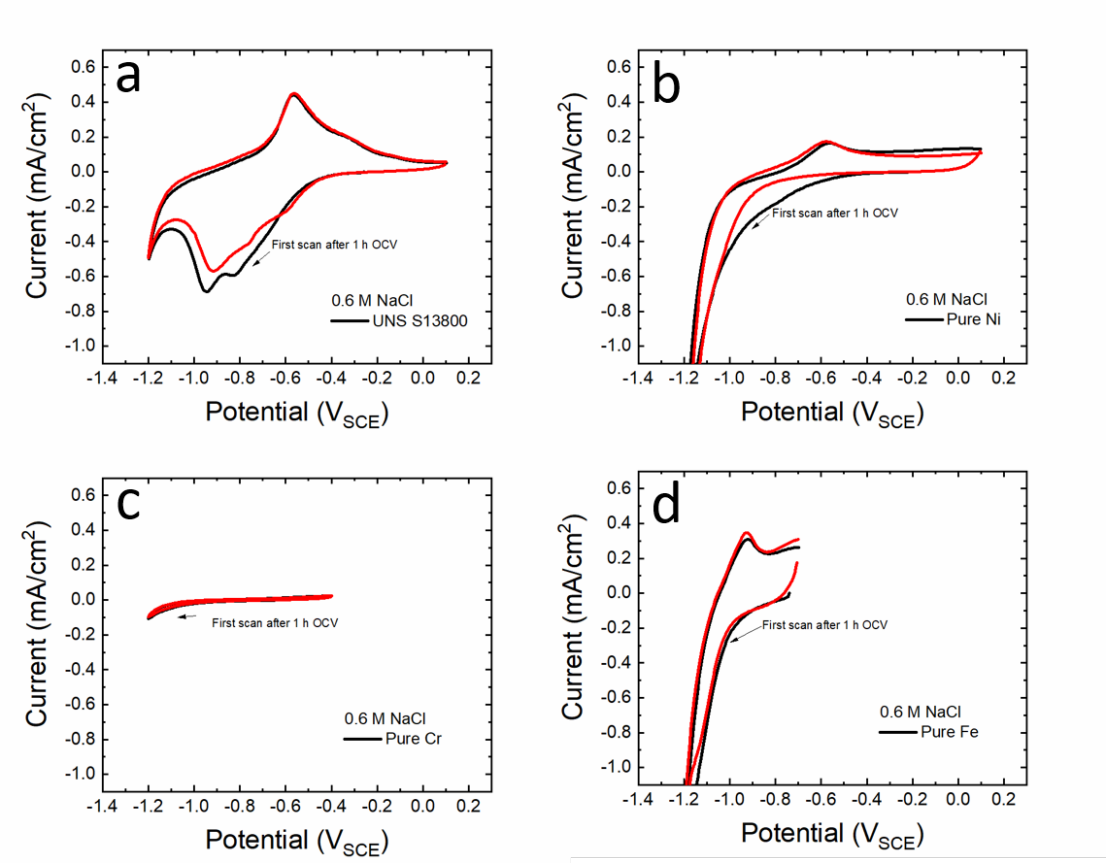

Figure 3 - Cyclic voltammograms for UNS S13800 and pure Ni, Cr and Fe coupons in 0.6 M NaCl (ambient aeration). Scan rate: 100 mV/s.

Figure 4 contains the same set of experiments as in Figure 3 but the solutions in these experiments have been deoxygenated by bubbling commercially pure Ar into the cell for the duration of the experiment. The main difference in this set of curves is observed in Figure 4a for UNS S13800. The UNS S13800 scans no longer have the ORR current as there is no oxygen in solution, however there also are no additional peaks in the -800 mV to -1000 mV region as in Figure 3a. The UNS S13800 OCP value is more negative in Ar, so the surface film is expected to change. A previous study by Piao et al. combined spectroscopic techniques to perform peak assignments for stainless steel (type 304) as well as Fe, Ni and Cr electrodes [23]. The main cathodic peak for UNS S13800 in Ar (Figure 4a) can be assigned to reduction of higher valence Fe oxide species to Fe^{2+} species. The corresponding anodic peaks are also less pronounced than in an oxygen environment, with one small peak at -650 mV.

Nickel (Figure 4b) shows the same behavior as in air, just without the ORR current on the first scan to more negative potentials. Chromium and iron show similar behavior in Ar as in air.

The increase in the peak height for the UNS S13800 in air could be due to a thicker redox-active oxide developed in the presence of oxygen and at a more positive OCP than in an Ar environment. Work by Marcelin et al. on UNS S13800 has shown that different oxides are produced in aerated versus deaerated solutions [10].

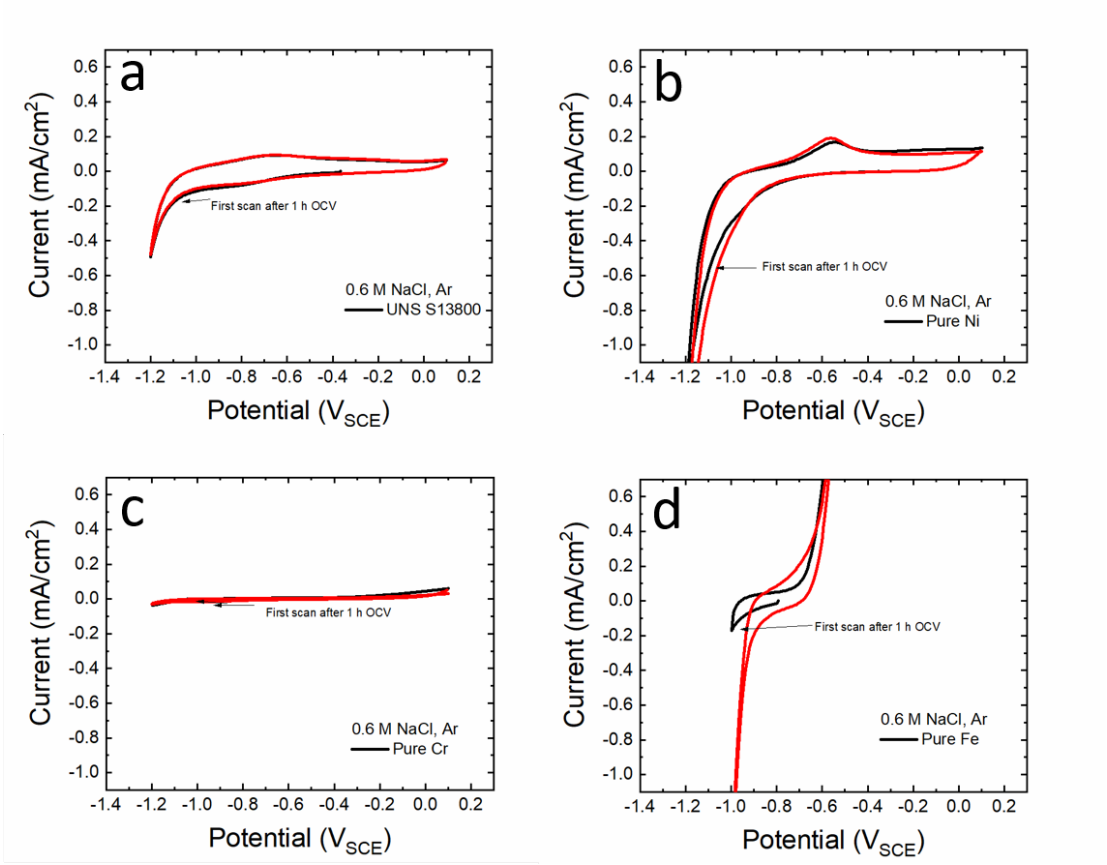

Figure 4 - Cyclic voltammograms for UNS S13800 and pure Ni, Cr and Fe coupons in 0.6 M NaCl in deoxygenated solution. Scan rate: 100 mV/s.

3.1.3 Potentiostatic EIS under ORR conditions

Pure chromium

A constant phase element (CPE) impedance model was used to fit the data and the resulting charge transfer resistance (R_p) values are listed in Tables 1 and 2. Oxide capacitance values were calculated using

[24], where C is the oxide film capacitance, Y_0 is the magnitude of the CPE, and α is an empirical constant to capture the deviation of the CPE from an ideal capacitor.

$$C = \frac{(Y_0 R_p)^{\frac{1}{\alpha}}}{R_p} \quad 1$$

:

Previous studies on well-defined FeOOH and Fe_3O_4 electrodes of the outer-sphere electron transfer reduction of ferricyanide highlight the importance of the conductivity of the passive film [9]. By using an outer-sphere redox couple that eliminated the surface specificity of the ORR it was found that in a rotating disk experiment that Fe_3O_4 only reached the diffusion-limited current at -400 mV, and on γ-FeOOH the reaction was completely inhibited. The differences in the oxidation states of the Fe ions on the surface was proposed as the explanation.

The potential dependence of the impedance is shown in Figure 5a for the FeCr sample and the fitting results in Table 1. Between -200 and -400 mV, there is little change in the capacitance, but once in the ORR region there is a large increase to 475 μF/cm^2. The capacitance decreases again once in the HER at -1200 mV. Pure chromium (Figure 5b) does not change until the HER region at -1200 mV.

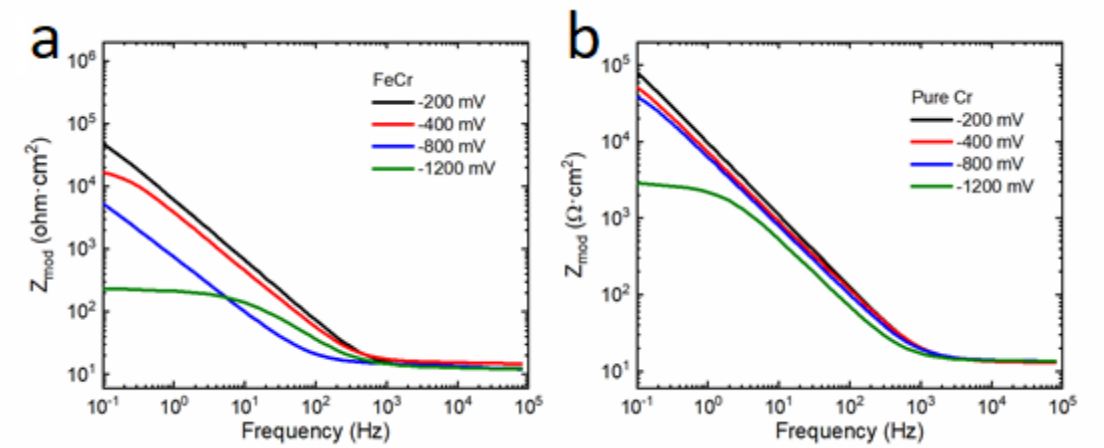

Figure 5 - Potentiostatic EIS spectra of a) FeCr thin film electrode after 1 h potentiostatic hold at indicated potentials and of b) bulk Cr electrode after 20 min potentiostatic hold at indicated potentials.

Table 1: Potentiostatic EIS Fitting Results for FeCr at different potentials in 0.6 M NaCl.

Potential	R_p (kΩ·cm^2)	Capacitance (μF/cm^2)
-200 mV	128	31
-400 mV	19	44
-800 mV	99	475
-1200 mV	0.2	84

Within the ORR region at -800 mV, the different materials are compared in Figure 6 and Table 2. The charge transfer resistance is lowest for Fe, and the capacitance of Cr is an order of magnitude lower than the stainless steel or FeCr samples. From the marked difference from pure Cr, the EIS data shows that the Fe is playing a role in the capacitance of the FeCr passive film. Importantly this behavior is similar to that of UNS S13800 stainless steel, even when other alloying elements are not included in the model alloy. Some difference is expected due to the difference in actual surface area between the sputtered films and the polished bulk metal coupons.

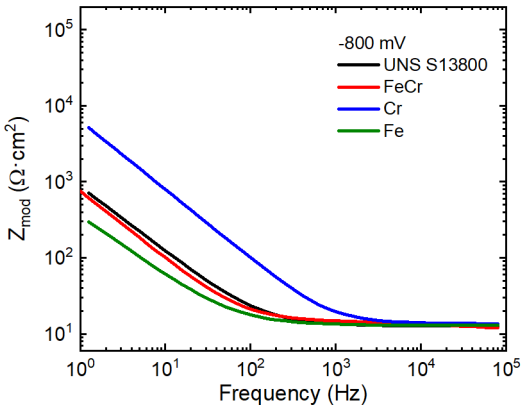

Figure 6 – Potentiostatic EIS spectra of UNS S13800, FeCr, pure Cr, and pure Fe at -800 mV in 0.6 M NaCl. FeCr was held for 1 h and all other materials for 20 min.

Table 2: Potentiostatic EIS Fitting Results at a potential of -800 mV in 0.6 M NaCl

Electrode	R_p ($k\Omega \cdot cm^2$)	*Capacitance* ($\mu F/cm^2$)
UNS S13800	42	364
FeCr	99	475
Cr	64	31
Fe	12	235

3.2 Surface Analysis

3.2.1 XPS

Figure 7 shows the XPS spectra for the Fe 2p edge for UNS S13800 and FeCr, for both the air-formed oxide as well as the 3600 s potentiostatic hold at -800 mV in 0.6 M NaCl. There is an increase in the contribution of the metal peak (707.0 eV) in the potentiostatically pretreated sample, as compared to the oxide/hydroxide peak at larger binding energies. However, the general similarity of the air and potentiostatic data are not surprising due to the *ex situ* nature of the experiment. The air oxide is expected to reform during the transfer from electrochemical cell to the vacuum chamber of the XPS instrument. The kinetics of formation of the air-formed oxide are rapid and there is a strong thermodynamic driving force for oxide formation after the oxide has been polarized to -800 mV and been, presumably, substantially thinned from its stable thickness. This further emphasizes the need for *in situ* chemical speciation measurements for reduced oxide films [11].

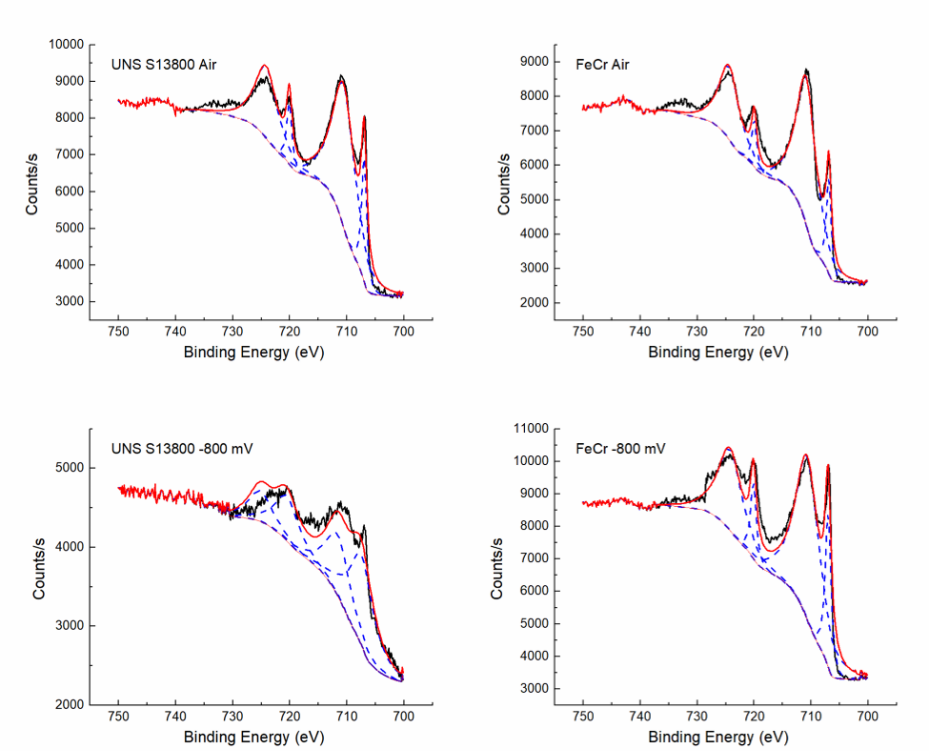

Figure 7 – High resolution XPS spectra of the Fe 2p region for UNS S13800 and the FeCr alloy.

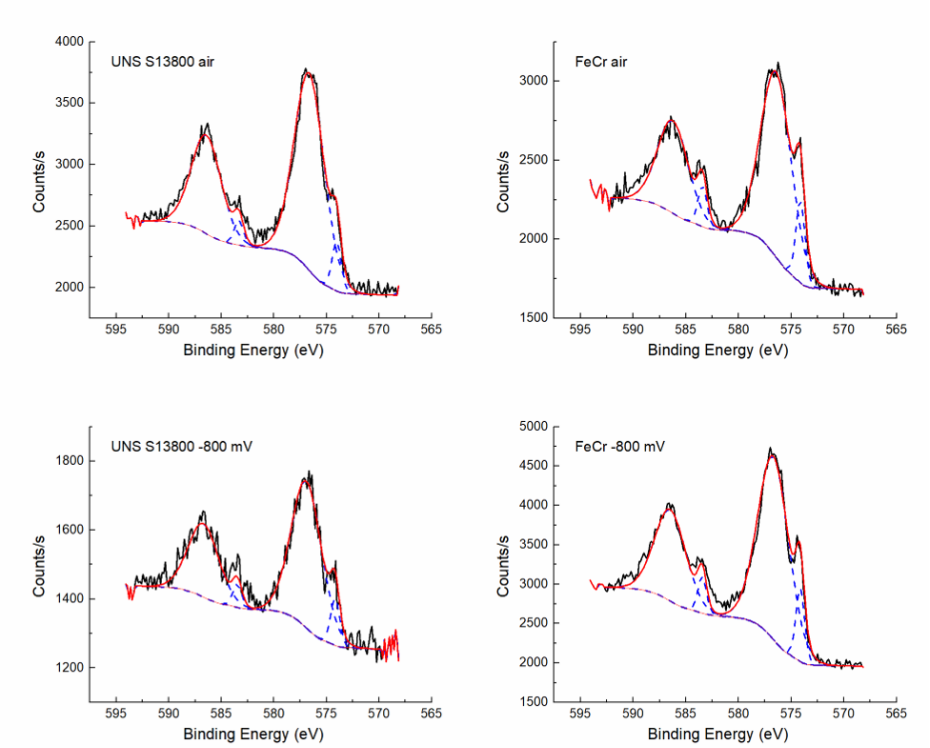

Figure 8 – High resolution XPS spectra of the Cr 2p region for UNS S13800 and the FeCr alloy.

3.2.2 GD-OES of Thin Film Electrodes

In order to more directly probe the main components of stainless steel, a model FeCr alloy was deposited as a thin film and used for analysis. Precise GD-OES measurements require a sample with a lower roughness than the features that will be measured. Because the passive films on stainless steels have thicknesses on the order of nanometers, usual surface metallography preparation is not adequate over the 4 mm diameter sampling size of that method to ensure that even sputtering occurs. To enable depth analysis, the FeCr model alloy was deposited onto a silicon wafer, and this surface was used in both electrochemical polarization experiments, as well as for the GD-OES analysis. It is within the first few nanometers where the passive film develops and changes with time, and it is in this region where composition information is the most valuable for understanding passive film evolution. By measuring the oxide film thickness, resistivity, and its chemical composition, the effect of each of these components can start to be understood. The measurement shown here in Figure 9 has the surface profiles for FeCr electrodes that have been only air-exposed, as well as two that were potentiostatically held at -400 mV and -800 mV. In all three profiles the surface oxide is evident, and the oxygen trace decays over the first 1-1.5 nm. Interestingly, the iron trace always begins below the bulk value, but then rises quickly at 1 nm. The chromium trace gradually increases from the surface inward, but then peaks above its bulk value, before reaching its steady bulk value of ~20 atomic percent. These results support a bilayer model where there is a chromium-rich inner layer at the interface between the oxide and the bulk metal. GD-OES has been previously used to study the surface oxide on a stainless steel (type 304) [25]. The surface Fe species was found to decrease when immersed in the H_2SO_4 solution in the study, and the Cr/Fe ratio increased in electrolyte-exposed samples. This is similar to what was observed here, despite the differences in electrolyte and conditions.

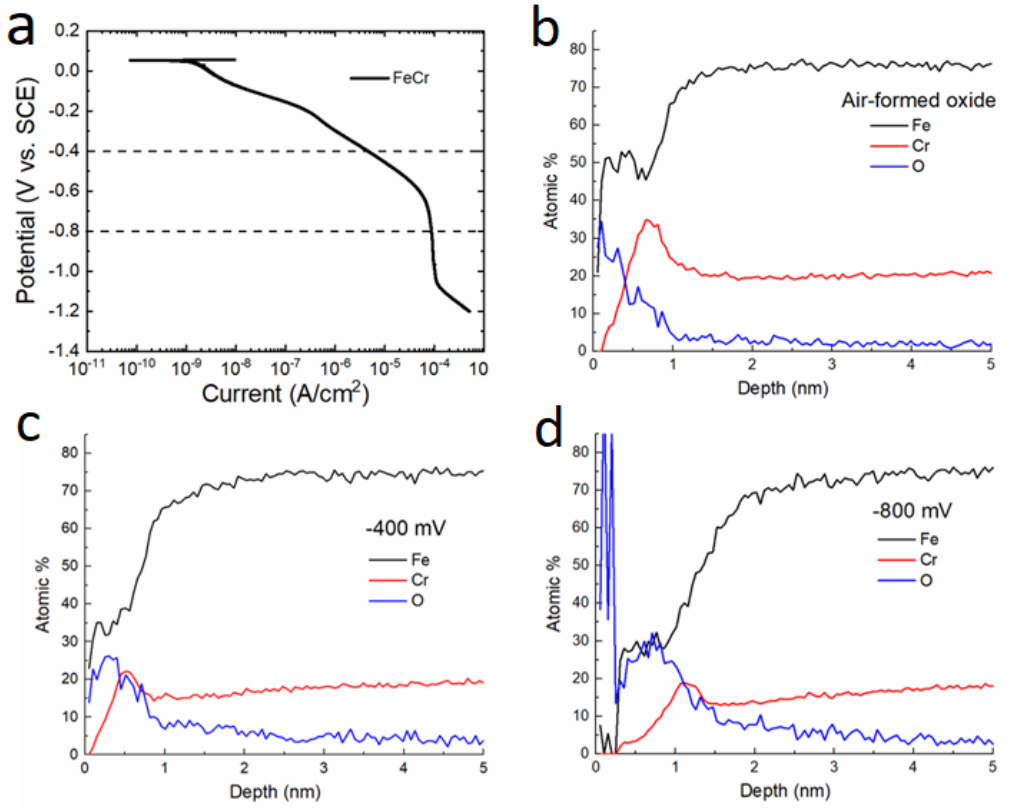

Figure 9 – a) Potentiodynamic scan of FeCr showing where the potential holds occurred for GD-OES analysis. GD-OES profiles of FeCr of b) the air-formed oxide, c) the FeCr after a potentiostatic hold at -200 mV, and d) FeCr after a potentiostatic hold at -800 mV.

3.3 XAS

3.3.1 Platinum Photocurrent X-ray Absorption Spectra

Figure 10 shows the *in situ* electrochemical cell. The working electrode was inserted through the back of the cell, leaving ~1 mm of space between the Kapton tape sealing the front of the cell and the surface of the electrode. The Pt counter electrode encircled the working electrode, and a reference electrode with a Luggin probe was placed in close proximity to the working electrode. The cell was placed at a 45° angle to the incident X-ray beam in order to collect fluorescence simultaneously with electrochemical data.

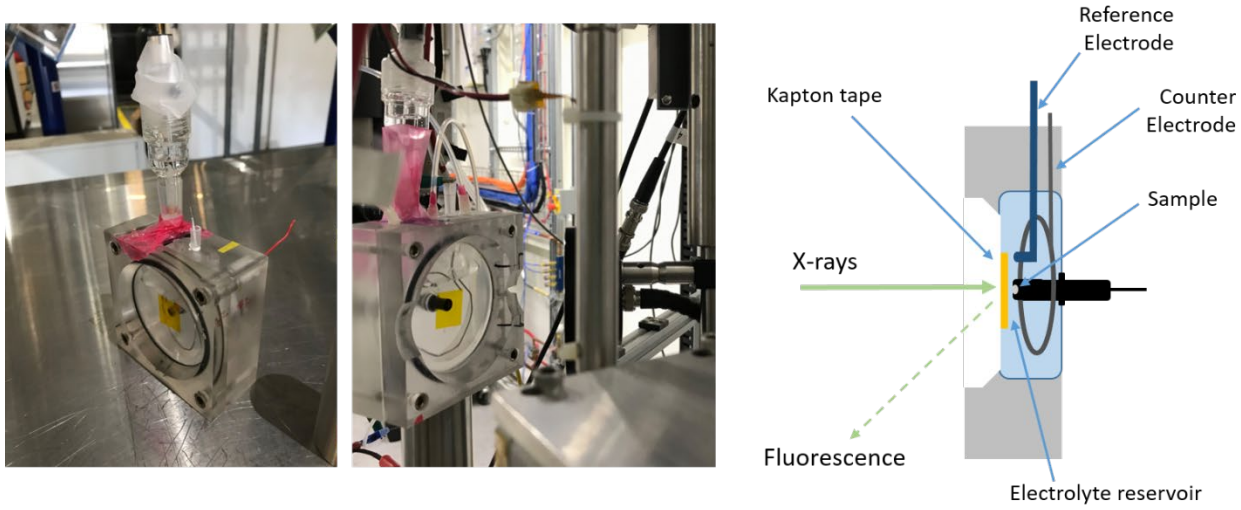

Figure 10 – Pictures and diagram of *in situ* electrochemical XAS cell.

As discussed in the Introduction, a new photocurrent XAS technique is demonstrated here. By measuring the current produced from the incident X-rays, electrochemical XAS data is produced in solution. Figure 11 shows the photocurrent overlaid on the fluorescence data of a bulk Pt electrode. The photocurrent experiment is a potentiostatic hold at -100 mV (in the double-layer region of Pt) This is an important proof-of-concept experiment to show the feasibility of this method.

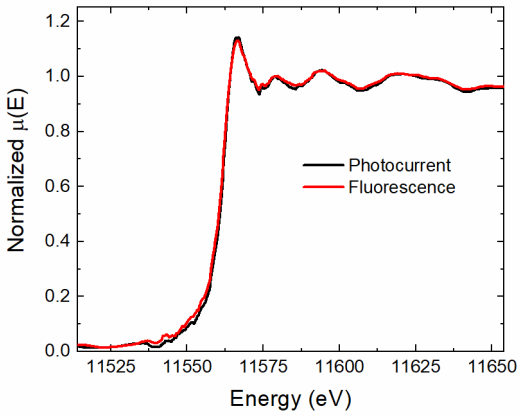

Figure 11 – In situ electrochemical XANES data at -100 mV for a bulk Pt electrode. The Pt L3 edge collected by the photocurrent technique is compared to fluorescence collection.

Previous XANES studies of FeCr materials used transmission mode to observe thin films. This ensures that even though the whole thickness is probed, the contribution of the surface is still significant. In these studies, a mix of Fe_2O_3 and Cr_2O_3 are deposited onto mylar tape [13]. In a borate buffer solution, it was found that at potentials starting at approximately -0.6 V_{sce} and up to -1.2 V_{SCE} there was a shift to lower energy of the edge position, indicating a change in oxidation state of the Fe edge. The initial shift was hypothesized to be a reduction from the +3 to +2 oxidation state. This potential region corresponds to the onset of ORR activity, further supporting the hypothesis that Fe^{2+} is the catalytically active component for ORR in stainless steel. There was no change in the chromium edge in scans from the OCP to -1.6 V_{SCE}. There has also been work on FeCr to show a decrease in step edge height in transmission mode, and, therefore, a decrease in concentration, of the Fe edge as the potential is held more negative. After a 1 hour hold at -1.4 V_{sce} in borate buffer a significant decrease in intensity was observed, most likely due to dissolution and chemical instability in this potential region. A small decrease in the Cr edge was also observed.

Initial studies of the UNS S13800 are presented in Figure 12. There is an increase in current at the Fe K edge (7112 eV), but the data are extremely noisy and no further information as to the speciation can be discerned. At these lower X-ray energies, the electrolyte is more absorbing and significant attenuation of the X-ray beam occurs. Much more can be learned from future *in situ* electrochemical XANES studies in which the potential is controlled while these preliminary XANES results shown here will inform future cell design and experimental methods in order to study bulk engineering alloys for *in situ* electrochemical experiments.

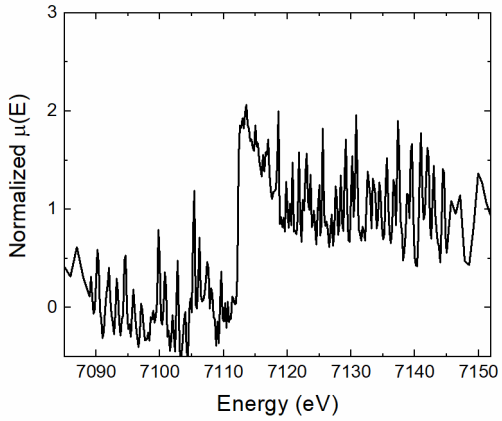

Figure 12 –Photocurrent Fe K edge XANES data of UNS S13800 held at -200 mV in 0.6 M NaCl.

4. CONCLUSIONS AND FUTURE WORK

From the EIS and potentiodynamic polarization experiments, the FeCr appears to be a good model alloy for stainless steel. Similar behavior was observed, even without the addition of other alloying elements, *e.g.* nickel. There is a coincident increase in the capacitance of the passive film and oxidation state change of the iron species occurring between -400 and -600 mV. This also corresponds to the expected reduction of the iron species in the oxide film from 3+ to 2+ charge state as evidenced by the XANES literature. Pure iron is not stable in that potential range, so a direct comparison is not possible. Only the iron species stabilized by the chromia layer can participate in ORR at those more positive potentials. The Fe^{2+} species have been hypothesized to be capable of binding molecular oxygen to

facilitate ORR [9, 26]. These studies suggest that iron oxide in some form, stabilized by chromium, is the important catalytic species and affects the capacitance of the oxide as a whole. If this relationship between oxidation state and ORR behavior can be better understood, a broad model for the ORR behavior of all stainless steels can be developed.

Future studies will include binary alloys of increasingly higher chromium content to determine if the change in current/impedance of the film are inversely related (and if this relationship is linear). In addition, separating the effect of the insulating film and the Fe species present on the surface would be an interesting approach. A noble metal electrode with a thin conformal layer of chromium deposited on the surface would provide the ability to determine the effect of the thin insulating layer on electron transfer kinetics. The next step would be to overcoat the Cr layer with a thin layer of Fe and see if tunneling is enhanced. In addition, the thickness/defective nature of the passive film needs to be separated from the role of the iron catalyst changing oxidation state. This could be done by using an outer-sphere electron transfer reaction, such as a common redox mediator. Ideally, this redox mediator would occupy the same potential region as that in which ORR occurs. Recent work from Bard and coworkers have studied the effect of thin metal oxide layers (tantalum and titanium) on the tunneling of electrons from an outer sphere redox mediator in solution [27]. Methods to remove the Fe species from the surface are also of interest to improve its galvanic corrosion properties. This would further passivate the stainless steel and suppress its ability to support cathodic reactions.

REFERENCES

1. Marcus, P., Surface science approach of corrosion phenomena. *Electrochimica Acta* **1998,** *43* (1), 109-118.
2. Olsson, C. O. A.; Landolt, D., Passive films on stainless steels—chemistry, structure and growth. *Electrochimica Acta* **2003,** *48* (9), 1093-1104.
3. Seyeux, A.; Maurice, V.; Marcus, P., Oxide Film Growth Kinetics on Metals and Alloys: I. Physical Model. *J. Electrochem. Soc.* **2013,** *160* (6), C189-C196.
4. Liu, C.; Srinivasan, J.; Kelly, R. G., Editors' Choice—Electrolyte Film Thickness Effects on the Cathodic Current Availability in a Galvanic Couple. *J. Electrochem. Soc.* **2017,** *164* (13), C845-C855.
5. Van den Steen, N.; Simillion, H.; Dolgikh, O.; Terryn, H.; Deconinck, J., An integrated modeling approach for atmospheric corrosion in presence of a varying electrolyte film. *Electrochimica Acta* **2016,** *187*, 714-723.
6. Matzdorf, C. A.; Nickerson, W. C.; Rincon Troconis, B. C.; Frankel, G. S.; Li, L. F.; Buchheit, R. G., Galvanic Test Panels for Accelerated Corrosion Testing of Coated Al Alloys: Part 1-Concept. *Corrosion* **2013,** *69* (12), 1240-1246.
7. Le Bozec, N.; Compère, C.; L'Her, M.; Laouenan, A.; Costa, D.; Marcus, P., Influence of stainless steel surface treatment on the oxygen reduction reaction in seawater. *Corrosion Science* **2001,** *43* (4), 765-786.
8. Moffat, T. P.; Yang, H.; Fan, F. R. F.; Bard, A. J., Electron-Transfer Reactions on Passive Chromium. *J. Electrochem. Soc.* **1992,** *139* (11), 3158-3167.
9. Vago, E. R.; Calvo, E. J.; Stratmann, M., Electrocatalysis of oxygen reduction at well-defined iron oxide electrodes. *Electrochimica Acta* **1994,** *39* (11), 1655-1659.
10. Marcelin, S.; Pébère, N.; Régnier, S., Electrochemical characterisation of a martensitic stainless steel in a neutral chloride solution. *Electrochimica Acta* **2013,** *87*, 32-40.
11. Bardwell, J. A.; Sproule, G. I.; Graham, M. J., Ex Situ Surface Analysis of Passive Films on Fe-Cr Alloys: When Is It Valid? *J. Electrochem. Soc.* **1993,** *140* (1), 50-53.
12. Davenport, A. J.; Sansone, M.; Bardwell, J. A.; Aldykiewicz, A. J.; Taube, M.; Vitus, C. M., *In situ* Multielement XANES Study of Formation and Reduction of the Oxide Film on Stainless Steel. *J. Electrochem. Soc.* **1994,** *141* (1), L6-L8.
13. Schmuki, P.; Virtanen, S.; Isaacs, H. S.; Ryan, M. P.; Davenport, A. J.; Böhm, H.; Stenberg, T., Electrochemical Behavior of Cr2 O 3 / Fe2 O 3 Artificial Passive Films Studied by *In situ* XANES. *J. Electrochem. Soc.* **1998,** *145* (3), 791-801.
14. Virtanen, S.; Schmuki, P.; Davenport, A. J.; Vitus, C. M., Dissolution of Thin Iron Oxide Films Used as Models for Iron Passive Films Studied by *In situ* X-Ray Absorption Near-Edge Spectroscopy. *J. Electrochem. Soc.* **1997,** *144* (1), 198-204.
15. Schroeder, S. L. M.; Moggridge, G. D.; Rayment, T.; Lambert, R. M., *In situ* probing of the near-surface properties of heterogeneous catalysts under reaction conditions: An introduction to total electron-yield XAS. *J. Mol. Catal. A: Chem.* **1997,** *119* (1), 357-365.
16. Erbil, A.; Cargill Iii, G. S.; Frahm, R.; Boehme, R. F., Total-electron-yield current measurements for near-surface extended x-ray-absorption fine structure. *Physical Review B* **1988,** *37* (5), 2450-2464.
17. Hansen, G. J.; O'Grady, W. E., A cell for x-ray absorption studies of the emersed electrochemical interphase. *Rev. Sci. Instrum.* **1990,** *61* (8), 2127-2132.
18. Schroeder, S. L. M.; Moggridge, G. D.; Ormerod, R. M.; Rayment, T.; Lambert, R. M., What determines the probing depth of electron yield XAS? *Surface Science* **1995,** *324* (2), L371-L377.
19. Tsuji, K.; Wagatsuma, K.; Sugiyama, K.; Hiraga, K.; Waseda, Y., EXAFS- and XANES-like spectra obtained by x-ray-excited scanning tunneling microscope tip current measurement. *Surface and Interface Analysis* **1999,** *27* (3), 132-135.

20. Tolmachev, Y. V.; Bae, I. T.; Scherson, D. A., X-ray Induced Photocurrents at the Metal/Solution Interface. *J. Phys. Chem. B* **2000,** *104* (32), 7663-7667.
21. Zečević, S.; Dražić, D. M.; Gojković, S., Oxygen reduction on iron: Part III. An analysis of the rotating disk-ring electrode measurements in near neutral solutions. *Journal of Electroanalytical Chemistry and Interfacial Electrochemistry* **1989,** *265* (1), 179-193.
22. Gojković, S. L.; Zečević, S. K.; Obradović, M. D.; DražIć, D. M., Oxygen reduction on a duplex stainless steel. *Corrosion Science* **1998,** *40* (6), 849-860.
23. Piao, T.; Park, S. M., Spectroelectrochemical Studies of Passivation and Transpassive Breakdown Reactions of Stainless Steel. *J. Electrochem. Soc.* **1997,** *144* (10), 3371-3377.
24. Brug, G. J.; van den Eeden, A. L. G.; Sluyters-Rehbach, M.; Sluyters, J. H., The analysis of electrode impedances complicated by the presence of a constant phase element. *Journal of Electroanalytical Chemistry and Interfacial Electrochemistry* **1984,** *176* (1), 275-295.
25. Deng, S.; Wang, S.; Wang, L.; Liu, J.; Wang, Y., Influence of Chloride on Passive Film Chemistry of 304 Stainless Steel in Sulphuric Acid Solution by Glow Discharge Optical Emission Spectrometry Analysis. *Int. J. Electrochem. Sci.* **2017,** *12*, 1106-1117.
26. Zagal, J.; Bindra, P.; Yeager, E., A Mechanistic Study of O_2 Reduction on Water Soluble Phthalocyanines Adsorbed on Graphite Electrodes. *J. Electrochem. Soc.* **1980,** *127* (7), 1506-1517.
27. Hill, C. M.; Kim, J.; Bodappa, N.; Bard, A. J., Electrochemical Nonadiabatic Electron Transfer via Tunneling to Solution Species through Thin Insulating Films. *Journal of the American Chemical Society* **2017,** *139* (17), 6114-6119.